JOURNAL OF MATERIALS SCIENCE 33 (1998) 4509–4516

Fatigue crack closure and crack growth behaviour in a titanium alloy with different microstructures

SHENG-HUI WANG, C. MÜLLER
Physical Metallurgy Division, Department of Materials Science, Darmstadt University of Technology, Petersenstr. 23, D-64287 Darmstadt, Germany

Fatigue crack closure and crack growth behaviour in Ti–2.5 wt % Cu alloy with two equiaxed and two lamellar microstructures have been investigated by constant-load amplitude tests. Plasticity-induced crack closure and roughness-induced crack closure have been characterized separately by experimental methods. A change in closure mechanism from plasticity-induced crack closure at high ΔK values (region of high stress intensity ranges) to roughness-induced crack closure at low ΔK values occurs in a solution-annealed equiaxed microstructure, while plasticity-induced crack closure is the operative closure mechanism in an over-aged equiaxed microstructure over the whole range of ΔK and roughness-induced crack closure occurs in two lamellar microstructures. The crack closing stress intensity factor for plasticity-induced crack closure increases continuously with increasing maximum stress intensity. The crack closing stress intensity factor for roughness-induced crack closure increases with increasing maximum stress intensity at low ΔK, and remains constant at high ΔK. Crack closure and crack path deflection have a significant influence on the crack growth rates.

1. Introduction

In most cases, three mechanisms can be taken into account concerning fatigue crack closure phenomena, i.e. plasticity-induced, roughness-induced and oxide-induced crack closure. Plasticity-induced crack closure, discovered by Elber [1, 2], is normally considered to arise from the development of residual plastic deformation remaining in the wake of an advancing crack. Roughness-induced crack closure is attributed to the crack path deflection, especially at the near-threshold range, at which a serrated or zigzag crack path is induced by microstructure-sensitive crack growth [3–5]. In this case, the kinked crack tip experiences a local mode II stress intensity, which may lead to significant mode II displacement and thus to wedge-closing at discrete contact points along the crack path. Oxide-induced crack closure is related to the role of excessive corrosion or fretting oxide debris [6], or associated with a thick oxidation layer [7], which causes wedge-closing of the crack at stress intensity factors above the minimum stress intensity. Oxide-induced crack closure may play a significant role at near threshold levels [8, 9] or at elevated temperature [10, 11]. Due to crack closure effects, the local crack driving force is reduced from the applied stress intensity range, ΔK ($\Delta K = K_{max} - K_{min}$, where K_{max} and K_{min} are maximum and minimum stress intensity factors in a fatigue load cycle, respectively), to an effective stress intensity range, ΔK_{eff} ($\Delta K_{eff} = K_{max} - K_{cl}$, where K_{cl} is the crack closing stress intensity factor).

While it is widely accepted that plasticity-induced crack closure is an important phenomenon during fatigue crack growth, especially under plane stress conditions, Vasudeven and co-workers [12, 13], from their studies based on dislocation theory, came to the conclusion that plastic deformation at crack tips is incapable of causing crack closure in the absence of any asperities. However, the elastic material surrounding the plastic zone may force displacements along the elastic–plastic boundary, promoting contact of the plastically stretched material and thus plasticity-induced crack closure without the need of fully reversed plastic strain [14]. Concerning plane strain cases, discrepancies in related literature about the existence of plasticity-induced crack closure are especially significant [15, 16]. It is difficult to imagine the origin of the "extra volume" of material in the crack flanks in plane strain (in contrast, in plane stress, the wedge of material in the crack path is easily envisaged to come from the side of the specimen). Nevertheless, plasticity-induced crack closure may arise from the "plasticity-induced wedge", resulting from the material transport along the crack growth direction due to plastic deformation at the crack tip [17]. Without local mode II displacement, this type of mismatch may, for example, be the misfit between "hills" and "valleys" of the two matching surfaces, or arise from micro-asperities induced by small crack branching [17].

Plasticity-induced closure may occur at all levels of stress intensity ranges [18]. Roughness-induced or oxide-induced crack closure, in contrast, play a predominant role only at near-threshold levels, especially under plane strain conditions [3]. The possible concurrence of the different types of crack closure makes

it difficult to separate their effects by experimental methods. The purpose of this paper is to present a detailed experimental study of crack closure mechanisms in a titanium alloy with various microstructures under plane strain conditions. Special attention is paid to the influence of the stress intensity factor range. The development of K_{cl} for roughness-induced crack closure and plasticity-induced crack closure with changing ΔK, as well as the effects of crack closure and crack path deflection on crack growth rates are discussed.

2. Experimental procedure

The material studied was a Ti–2.5 wt % Cu alloy, which was available as a solution-annealed bar (diameter 120 mm) as well as a hot rolled and stress-relieved plate (thickness 10 mm). Test specimens were in two as-received conditions machined from the bar and the plate, respectively, and two heat-treated conditions using the plate material. After ageing at 400 °C for 8 h, followed by ageing at 475 °C for 8 h, the material is in an under-aged condition [19]. After hot-rolling and stress-relief treatment the material is over-aged (ensured by a final ageing). The heat treatments used and the resulting characteristics of the microstructures are listed in Table I. The microstructures are shown in Fig. 1. The mean grain size and the mean lamellae colony size were measured by the linear intercept method [20] on optical micrographs. The lamella width was measured perpendicular to the longest direction of the lamella cross-sections. Tensile testing was conducted using cylindrical specimens with a gauge length of 15 mm and a diameter of 4 mm. The tensile direction was perpendicular to the rolling direction for specimens taken from the plate, and parallel to the radial direction for specimens taken from the cylindrical bar. The microstructural data and the mechanical properties are listed in Tables II and III, respectively.

Compact tension (CT) specimens with a width of 30 mm and a thickness of 8 mm were used for fatigue testing. The orientation of the crack plane was chosen

TABLE I Microstructural characteristics and heat treatments

Microstructural characteristics	Heat treatment	Micrograph
Equiaxed over-aged (EQO)	Annealed and stress relieved + A[a]	Fig. 1a
Equiaxed (EQ)	Solution annealed	Fig. 1b
Coarse lamellar aged (CL), lamellae packages	920 °C 0.5 h $\xrightarrow{1\ \mathrm{K\ min^{-1}}}$ 805 °C 0.5 h/WQ[b] + A[a]	Fig. 1c
Fine lamellar aged (FL), Widmanstätten type	920 °C 0.5 h/WQ[b] + 805 °C 0.5 h/WQ[b] + A[a]	Fig. 1d

[a]A: aged for 8 h at 400 °C and 8 h at 475 °C.
[b]WQ: water quenched.

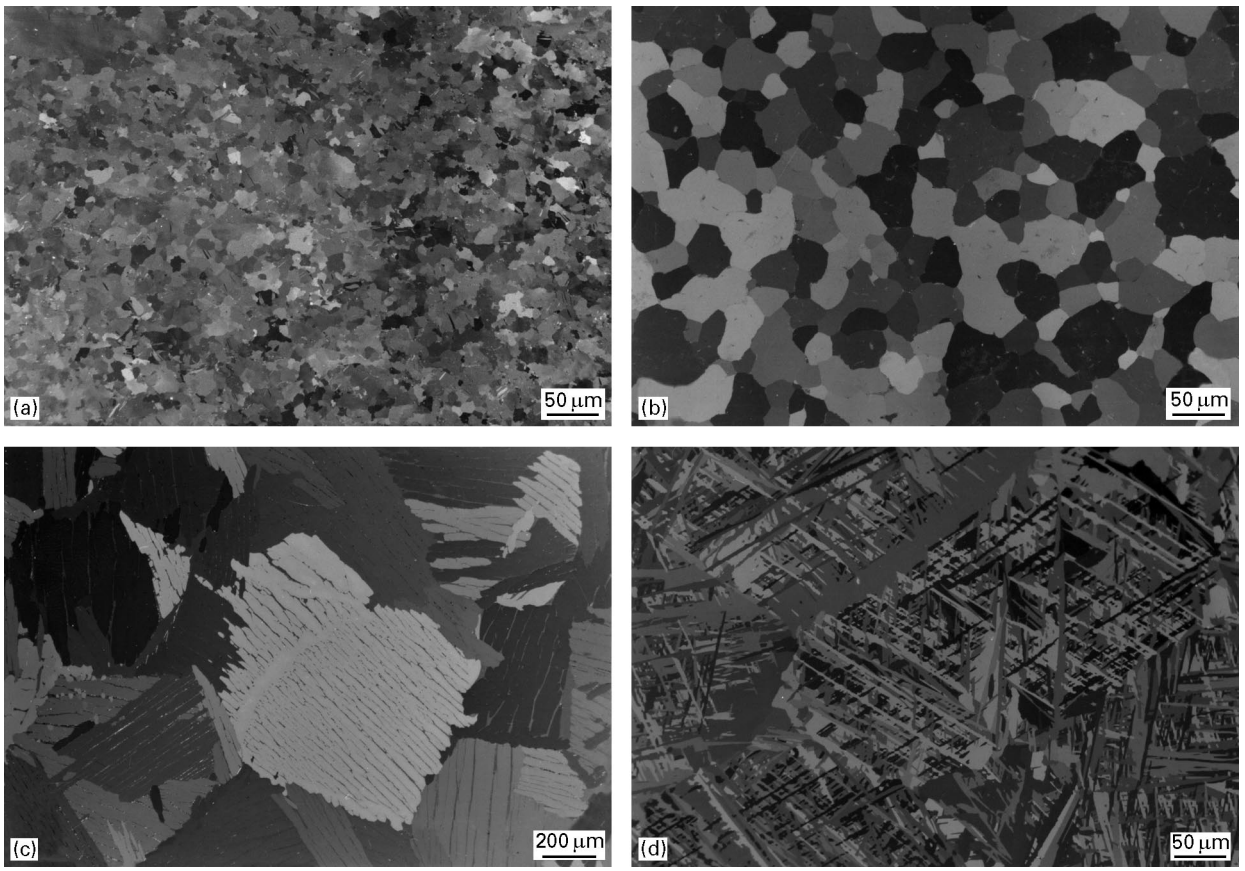

Figure 1 Microstructures of Ti–2.5 wt % Cu alloy: (a) over-aged equiaxed (EQO), (b) solution-annealed equiaxed (EQ), (c) coarse lamellar (CL) and (d) fine lamellar (FL).

TABLE II Microstructural data for different microstructures

	Mean α grain size (μm)	Mean prior β grain size (μm)	Mean lamellar colony size (μm)	Maximum lamella length (μm)	Lamella width (μm)
EQO	17	–	–	–	–
EQ	43	–	–	–	–
CL	–	–	580	1650	37
FL	–	312	–	1200[a]	4.4

[a]Maximum prior β grain size.

TABLE III Mechanical properties of the material with different microstructures

	Yield strength, $R_{p0.2}$ (MPa)	Ultimate tensile strength, R_m (MPa)	True fracture stress, σ_F (MPa)	Elongation to rupture, A (%)	Reduction of area, Z (%)
EQO	522	594	738	24.5	39
EQ	516	598	984	28	46
CL	600	723	838	13.5	15
FL	713	832	1080	17	25

to be R–C (see ASTM standard E 399-74) for the specimen taken from the bar and T–L for specimens taken from the plate. Fatigue crack growth testing was performed on a Schenck servo-hydraulic testing machine at room temperature in laboratory air. Tests were conducted under load control with a cyclic frequency of 30 Hz (sine wave) and a load ratio, R, of 0.1. The crack length was measured with a travelling microscope, with an accuracy of 0.01 mm. A load-shedding technique was used to determine the fatigue threshold, ΔK_{th}, defined as the stress intensity range at a crack growth rate, da/dN, of about 1×10^{-10} m cycle^{-1}.

After the fatigue threshold was reached by the load-shedding process, a constant-load-amplitude test was carried out to study fatigue crack growth and crack closure behaviour. The crack closing intensity factor, K_{cl}, was determined by a compliance technique with a cyclic frequency of 0.3 Hz. A crack mouth gauge was used to measure the change of crack mouth opening displacement with applied load. An offset procedure was used for better determination of the crack closing load [21, 22]. K_{cl} was determined after each crack length increment of about 0.25 mm.

The fracture surfaces were investigated using a scanning electron microscope. One-half of the fractured specimen was vertically sectioned through the fracture surface (parallel to the crack propagation direction) for crack path observations. Roughness prameters (the standard deviation of the height, S_H, and the standard deviation of angular distribution, S_θ) were quantified by digitizing the crack profile using an image analyser as described in detail in an earlier paper [23].

3. Results and discussion

3.1. Influence of crack closure and crack path deflection on crack growth rates

Significant crack closure is measured in all the microstructures. K_{cl} measured during constant-load-amplitude tests is compared for the different microstructures in Fig. 2. Larger K_{cl} is observed in lamellar microstructures (CL and FL) than in equiaxed microstructures (EQ and EQO).

The crack growth rates appear to be lower in lamellar microstructures than in equiaxed microstructures as shown in Fig. 3 (represented in terms of ΔK). The highest crack growth rates are observed in EQO and the lowest in CL. The difference in crack growth rates is, in part, attributed to crack closure effect. When da/dN is represented in terms of ΔK_{eff} as shown in Fig. 4, the difference in crack growth rates becomes significantly smaller.

In addition to crack closure, crack path deflection has an influence on crack growth rates. Fig. 5 shows the results of quantitative analysis of the crack path profile. The standard deviation of the height distribution, S_H, and the standard deviation of the angular distribution, S_θ, are used to describe a crack path profile as proposed by Wasén *et al.* [24]. S_H is correlated to the average roughness height, while S_θ is a measure of the mean tilt angles of the crack path [22–24]. Large S_H and S_θ, indicating strong crack path deflection, are found in lamellar microstructures (especially in CL), while in EQO, S_H and S_θ are small, in correlation with a linear crack path. In EQ, S_H and S_θ are large at low ΔK values related to a highly serrated crack path, and small at high ΔK values related to a linear crack path. In Fig. 4, the lower crack growth rates in EQ at low ΔK may be attributed to a strongly deflected crack path in contrast to the linear crack path in EQO. A deflected crack tip results in a reduction of the local driving force for crack propagation, and crack path deflection causes an increase in the total length of the crack path from a microscopic point of view. Thus, stronger crack path deflection results in lower nominal crack growth rates [25–28]. CL and FL experience strong crack deflection but show almost identical crack growth rates as EQO in Fig. 4. According to the above consideration, it can be reasonably assumed that lamellar microstructures

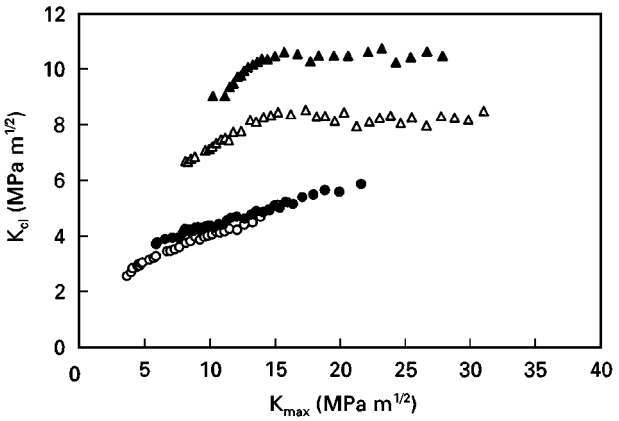

Figure 2 Variation of K_{cl} with K_{max} in different microstructures. ○ EQO; ● EQ; △ FL; ▲ CL.

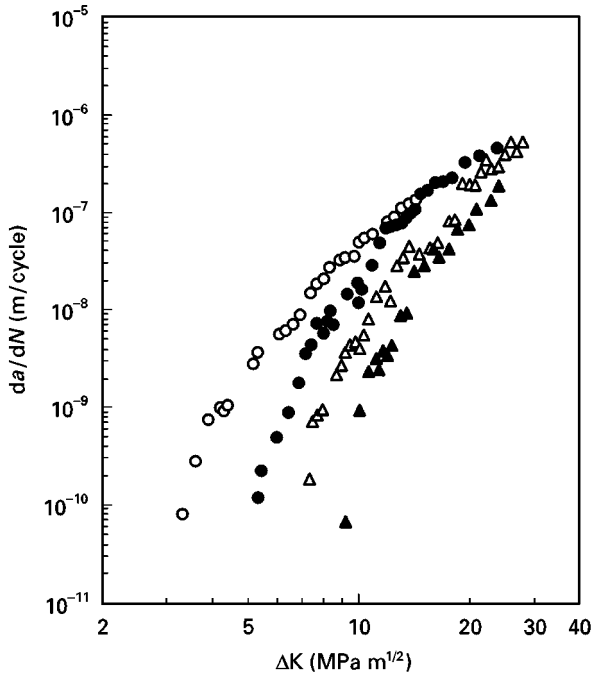

Figure 3 Variation of fatigue crack growth rate, da/dN, with nominal stress intensity range, ΔK, in different microstructures. ○ EQO; ● EQ; △ FL; ▲ CL.

experience higher intrinsic crack growth rates (with the effects of crack closure and crack path deflection being eliminated) than equiaxed microstructures.

3.2. Plasticity-induced crack closure

For equiaxed over-aged microstructures (EQO), highly linear crack paths and heavily plastically deformed fracture surfaces are observed both at high ΔK (Fig. 6a) and at low ΔK (Fig. 6b). Crystallographic fracture is not observed, even at the near-threshold range. This is attributed to the slip-homogenizing effect of non-shearable incoherent Ti_2Cu precipitates, which act as deformation barriers in addition to grain boundaries promoting cross slip, similar to the effect of precipitates in aluminium alloys [29]. As shown in Fig. 5, S_H and S_θ for EQO are small, remaining almost constant with changing K_{max}. The small scale of fracture surface roughness is attributed to micro-asperities due to plastic deformation at the crack tip. The crack

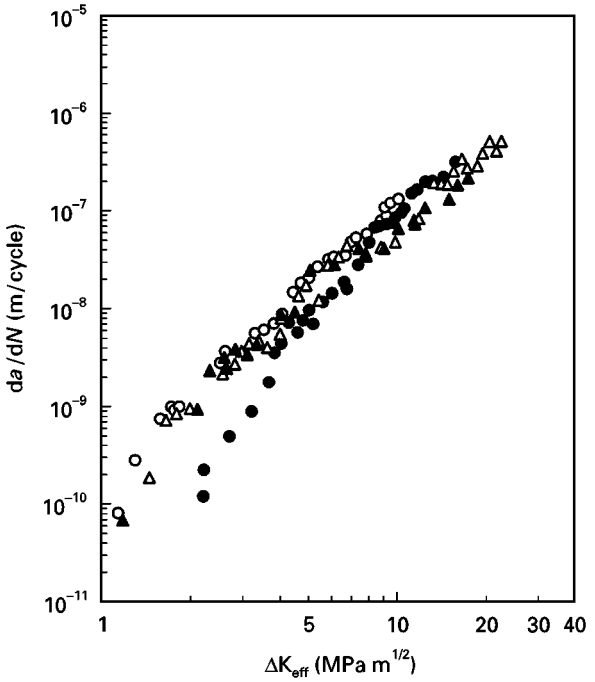

Figure 4 Variation of fatigue crack growth rate, da/dN, with effective stress intensity range, ΔK_{eff}, in different microstructures. ○ EQO; ● EQ; △ FL; ▲ CL.

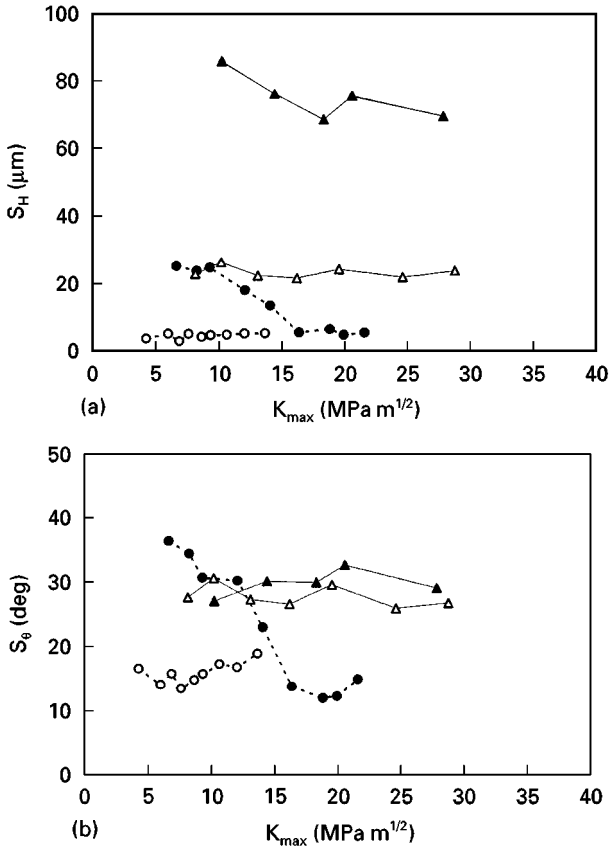

Figure 5 Variation of (a) standard deviation of height distribution, S_H, and (b) standard deviation of angle distribution, S_θ, with K_{max} in different microstructures. —○— EQO; —●— EQ; —△— FL; —▲— CL.

closure induced by these micro-asperities of plastic deformation (the material being plastically stretched in a direction perpendicular to the fracture surface) should be referred to as plasticity-induced crack closure, rather than roughness-induced crack closure due

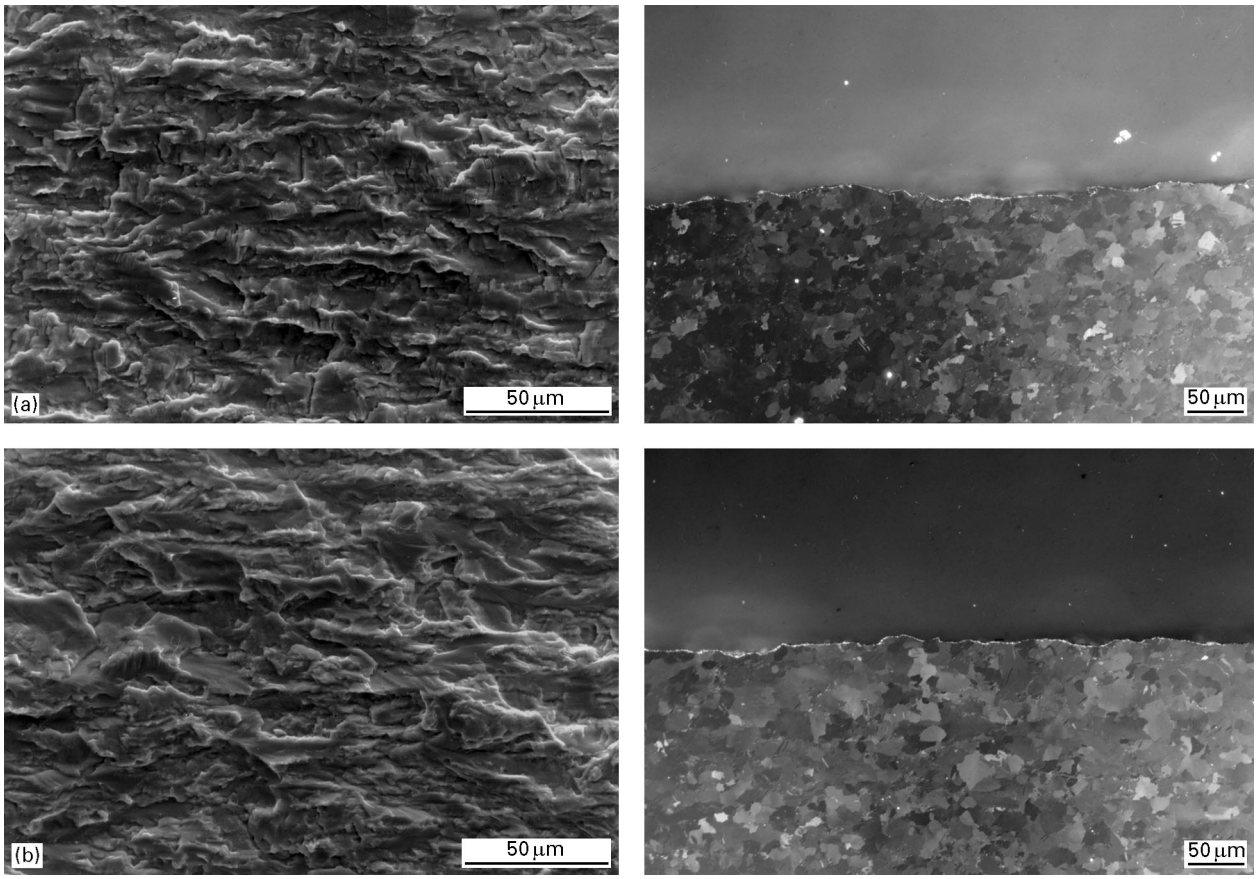

Figure 6 Fatigue fracture surfaces (scanning electron micrographs) and corresponding crack path morphologies (optical micrographs, polarized light) of EQO at (a) $\Delta K = 16\ \mathrm{MPa\,m^{1/2}}$ and (b) $\Delta K_{th} = 3.3\ \mathrm{MPa\,m^{1/2}}$ (crack growth from left to right).

to the lack of a tortuous crack path. This indicates that plasticity-induced crack closure is the operative closure mechanism over the whole range of ΔK for EQO. In this case, K_{cl} increases continuously with increasing K_{max} (Fig. 2).

It should be noted that oxide-induced crack closure can be excluded, as no fretting debris are observed on the fracture surface and the formation of a thick oxide film on the fracture surface is not possible during room temperature testing of titanium alloys.

3.3. Roughness-induced crack closure

For lamellar microstructures (CL and FL) at low ΔK, cleavage-like fracture surfaces and tortuous crack paths, correlated with planar slip, are observed (as shown for CL in Fig. 7a). Due to planarity of slip, the crack propagates along the crystallographic plane, not resulting in the material being plastically stretched in the direction perpendicular to the crack plane. Therefore, roughness-induced crack closure is the operative mechanism in lamellar microstructures at low ΔK.

At high ΔK, a highly tortuous crack path is observed in lamellar microstructures as well, despite a somewhat ductile fracture surface (as shown for CL in Fig. 7b). As shown in Fig. 2, K_{cl} for CL and FL lacks any significant change with changing K_{max} (while the change of K_{cl} with K_{max} is typical for plasticity-induced crack closure) and is much higher than that for equiaxed microstructures with heavy plastic deformation. Thus, rather than plasticity-induced crack closure, roughness-induced crack closure prevails here.

Quantitative analysis of the crack path profile confirms that, over the whole range of ΔK, there are highly tortuous crack paths in lamellar microstructures. As shown in Fig. 5, S_H and S_θ are large for CL and FL, much larger than those for EQO, over the whole range of ΔK, remaining almost constant with changing K_{max}.

A change in the development course of K_{cl} for roughness-induced crack closure with increasing K_{max} in lamellar microstructures is found to be correlated with the change in fracture mode at ΔK_{tr} (Fig. 8). The transition in fracture mode is discussed in an earlier paper in detail [30]. At low ΔK ($\Delta K < \Delta K_{tr}$), planar slip prevails. Higher K_{max} results in larger local mode II displacement, and in a larger irreversible mode II displacement upon unloading, causing higher K_{cl} [22, 31]. At high ΔK levels ($\Delta K > \Delta K_{tr}$), secondary slip takes place, although fracture still proceeds mainly along the primary slip planes [22, 30]. At higher K_{max} more secondary cross slip systems are active. However, secondary cross slip has no contribution to net mode II displacement (the secondary slip along the slip plane with a tilt angle of θ is counteracted by one with a tilt angle of $-\theta$). Mode II displacement is saturated at a constant level. Therefore, K_{cl} does not increase despite increasing K_{max} in this range.

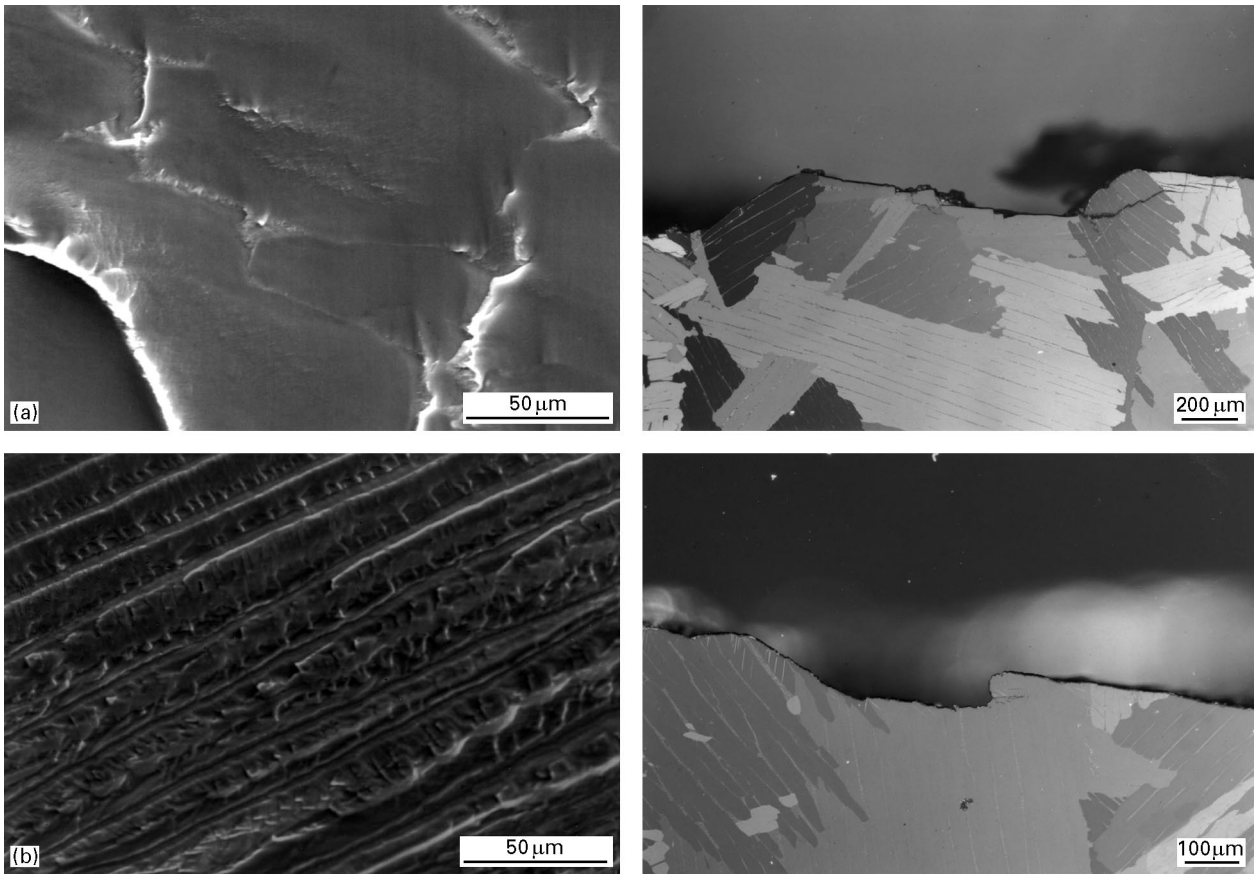

Figure 7 Fatigue fracture surfaces (scanning electron micrographs) and corresponding crack path morphologies (optical micrographs, polarized light) of CL at (a) $\Delta K_{th} = 9.2\ \mathrm{MPa\,m^{1/2}}$ and (b) $\Delta K = 25\ \mathrm{MPa\,m^{1/2}}$ (crack growth from left to right).

3.4. Transition crack closure mechanism with changing ΔK

In contrast to EQO, the solution-annealed equiaxed microstructure (EQ) experiences a fracture mode change at ΔK_{tr} [30]. At high ΔK ($\Delta K > \Delta K_{tr}$), a highly linear crack path and heavily plastically deformed fracture surfaces are observed (Fig. 9a). As in EQO, plasticity-induced crack closure is the operative crack closure mechanism in EQ at high ΔK. At low ΔK ($\Delta K < \Delta K_{tr}$), crystallographic facets coexist with ductile fracture regions, and large facets result in significant crack deflection in EQ (Fig. 9b). Thus, roughness-induced crack closure is the operative mechanism in EQ at low ΔK.

This change of crack path features associated with a fracture mode change is also reflected by the roughness parameters of the crack path profile. S_H and S_θ in EQ remain small with changing K_{max} at high ΔK, while both increase significantly with decreasing K_{max} at low ΔK (Fig. 5). At near-threshold, S_H is at the same level as that of FL, and S_θ is higher than that of CL and FL.

Plasticity-induced crack closure for EQ and EQO at high ΔK ($\Delta K > \Delta K_{tr}$) has the same value of K_{cl} (Fig. 10), due to similar mechanical properties. At low ΔK, however, K_{cl} is higher in EQ than that of plasticity-induced crack closure in EQO at the same stress-intensity range (Fig. 10). This observation is attributed to pronounced crack path deflection and thus to roughness-induced crack closure in EQ at low ΔK. Nevertheless, the K_{cl} in EQ at the near-threshold level is much lower than that of FL (Fig. 2), despite the same level of S_H and an even higher S_θ (Fig. 5). This might be attributed to the ductile fracture regions observed [23]. As ductile fracture at the crack tip does not result in local mode II displacement, mode II displacement along the planar facets nearby, and thus the overall mode II displacement along the crack front, is restricted, resulting in a low K_{cl} in EQ.

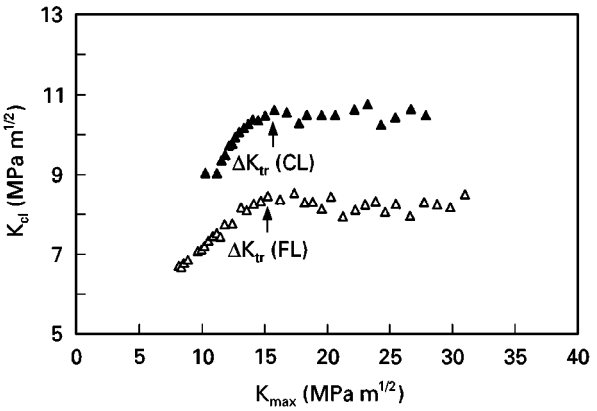

Figure 8 Development of roughness-induced crack closure in lamellar microstructures. △ FL; ▲ CL.

3.5. Crack closure ratio

The closure ratio, K_{cl}/K_{max}, used in the literature to describe the crack closure level, decreases with increasing K_{max} for both plasticity-induced and

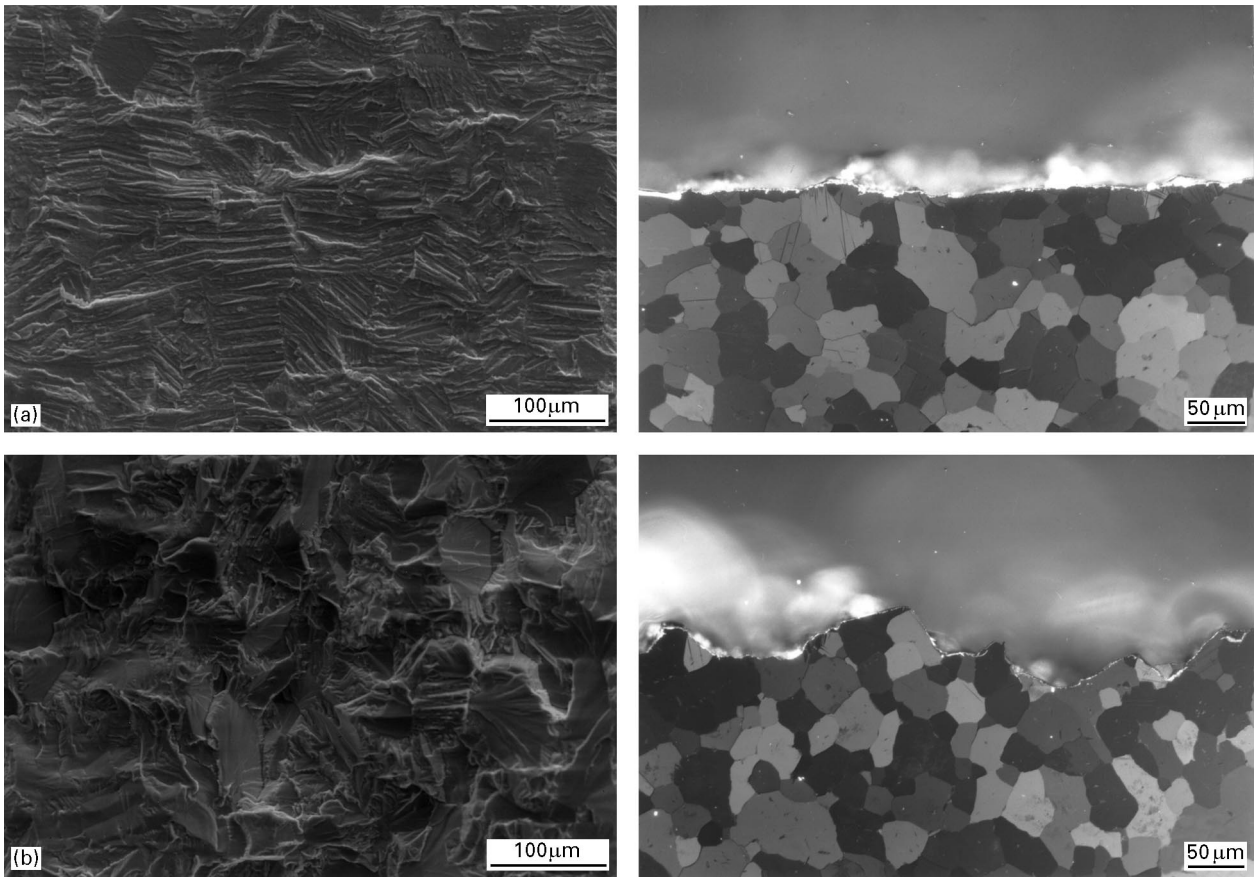

Figure 9 Fatigue fracture surfaces (scanning electron micrographs) and corresponding crack path morphologies (optical micrographs, polarized light) of EQ at (a) $\Delta K = 20\ \mathrm{MPa\,m^{1/2}}$ and (b) $\Delta K_{th} = 5.3\ \mathrm{MPa\,m^{1/2}}$ (crack growth from left to right).

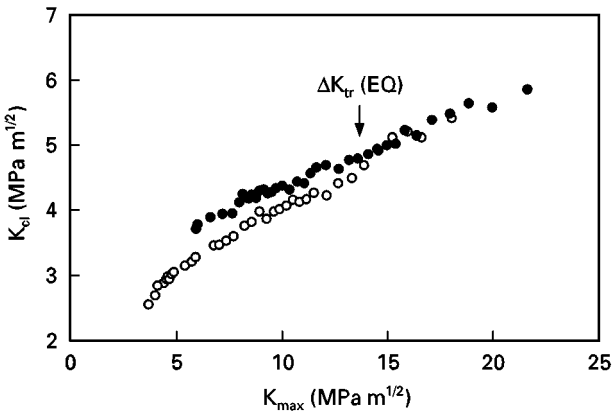

Figure 10 Comparison between changes of K_{cl} with K_{max} in equiaxed microstructures, EQ and EQO. ○ EQO; ● EQ

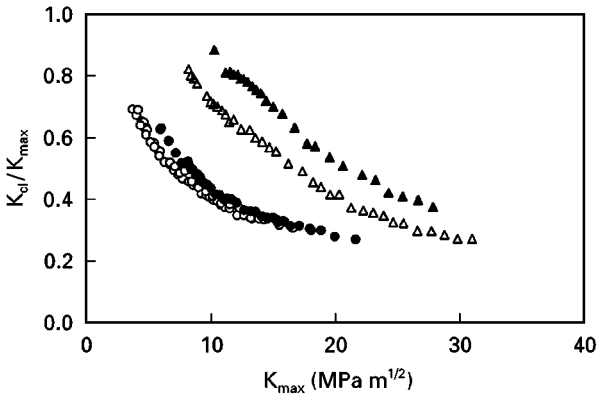

Figure 11 Relationship between K_{cl}/K_{max} and K_{max} in different microstructures. ○ EQO; ● EQ; △ FL; ▲ CL.

roughness-induced crack closure (Fig. 11). Plasticity-induced crack closure is the operative mechanism in EQO, not only at high ΔK but also at low ΔK values; nevertheless, the K_{cl}/K_{max} increases with decreasing ΔK. This observation is in agreement with the numerical results of McClung and Sehitoglu [32], but disagrees with the common view that K_{cl}/K_{max} is constant for plasticity-induced crack closure [18, 33] and that the increase in K_{cl}/K_{max} with decreasing K_{max} at the low ΔK level is due to roughness-induced crack closure [34, 35].

4. Conclusions

1. Depending on microstructural features, titanium alloy may experience a change in crack closure mechanism with changing ΔK (e.g. from plasticity-induced crack closure at high ΔK to roughness-induced crack closure at low ΔK in the solution-treated equiaxed microstructure), or only experience plasticity-induced crack closure (in the fine grained over-aged equiaxed microstructure) or roughness-induced crack closure (in the lamellar microstructures) both at low ΔK and at high ΔK.

2. Crack closure has a significant influence on fatigue crack growth rates. In addition, crack path deflection is an important factor that affects crack growth rates.

3. For plasticity-induced crack closure, K_{cl} increases continuously with increasing K_{max}. For roughness-induced crack closure, K_{cl} increases with increasing K_{max} at low ΔK associated with planar slip, and remains constant at high ΔK level due to the influence of secondary cross slip.

4. The crack closure ratio, K_{cl}/K_{max} increases with decreasing ΔK for both plasticity-induced crack closure and roughness-induced crack closure. It cannot be assumed that the increase in crack closure ratio with decreasing ΔK at near-threshold level is attributed to roughness-induced crack closure without detailed study of the crack closure mechanism.

Acknowledgements

The authors would like to express their sincere gratitude to Professor H. E. Exner for his stimulating discussions and constructive criticism during the investigation, as well as useful comments on the manuscript.

References

1. W. ELBER, *Engng Fracture Mech.* **2** (1970) 37.
2. *Idem*, in "Damage Tolerance in Aircraft Structures", ASTM STP 486 (American Society for Testing and Materials, Philadelphia, PA, 1971) p. 230.
3. S. SURESH, in "Plastic Deformation and Fracture of Materials", Materials Science and Technology, Vol. 6, edited by R. W. Cahn, P. Haasen and E. J. Kramer (VCH Verlagsgesellschaft mbH, Weinheim, 1993) p. 281.
4. R. O. RITCHIE and S. SURESH, *Metall. Trans. A* **13A** (1982) 937.
5. S. SURESH and R. O. RITCHIE, *ibid.* **13A** (1982) 1627.
6. S. SURESH, G. F. ZAMISKI and R. O. RITCHIE, *ibid* **13A** (1982) 1627.
7. H. KOBAYASHI, H. TSUJI and K. D. PARK, in "Fracture and Strength '90", Key Engineering Materials, Vols 51 and 52, edited by K. Y. Lee and H. Takahashi (Trans Tech Publications, Zürich, 1990) p. 355.
8. P. K. LIAW, T. R. LEAX, R. S. WILLIAMS and M. G. PECK, *Metall. Trans. A* **13A** (1982) 1607.
9. S. DHAR, in "*Fatigue '90*", edited by H. Kitagawa and T. Tanaka (Materials and Component Engineering Publications Ltd, Birmingham, 1990) p. 1261.
10. P. J. COTTERILL and J. F. KNOTT, *Acta Metall. Mater.* **40** (1992) 2753.
11. L. P. ZAWADA and T. NICHOLAS, in "Fracture Mechanics: Eighteenth Symposium", ASTM STP 945, edited by D. T. Read and R. P. Reed (American Society for Testing and Materials, Philadelphia, PA, 1988) p. 192.
12. A. K. VASUDEVAN, K. SADANANDA and N. LOUAT, *Mater. Sci. Eng.* **A188** (1994) 1.
13. N. LOUAT, K. SADANANDA, M. DUESBERY and A. K. VASUDEVAN, *Metall. Trans. A* **24A** (1993) 2225.
14. J. D. DOUGHERTY, T. S. SRIVATSAN and J. PADOVAN, *Engng Fracture Mech.* **56** (1997) 167.
15. R. RIPPIN, C. BICHLER, C. SOMMITSCH and O. KOLEDNIK, in "Fatigue *'96*", edited by G. Lütjering and H. Nowack (Elsevier Science, Oxford, 1996) p. 411.
16. R. C. McCLUNG, B. H. THACKER and S. ROY, *Int. J. Fracture* **50** (1991) 27.
17. R. PIPPAN, O. KOLEDINK and M. LANG, *Fatigue Fracture Engng Mater. Struct.* **17** (1994) 721.
18. K. ASAMI, in "Fractography", Current Japanese Materials Research, Vol. 6, edited by R. Koterazawa, R. Ebara and S. Nishida (Elsevier Applied Science, Ltd, 1990) p. 1.
19. P. A. BLENKINSOP and R. E. GOOSEY, in "The Science, Technology and Application of Titanium", edited by R. I. Jaffee and N. E. Promisel (Pergamon Press, Oxford, 1970).
20. H. E. EXNER, *Pract. Metallogr.* **30** (1993) 287.
21. N. A. FLECK, The use of compliance and electrical resistance techniques to characterise fatigue crack closure, Report No. CUED/C/MATS/TR89, (Department of Engineering, Cambridge University, Cambridge, 1982).
22. S.-H. WANG, PhD thesis, Technical University of Darmstadt, Germany, (1997).
23. S.-H. WANG and C. MÜLLER, *Mater. Sci. Eng. A* (1998) in press.
24. J. WASÉN, B. KARLSSON and K. HAMBERG, *Acta Stereol.* **6** (1987) 199.
25. S. SURESH, *Metall. Trans. A* **14A** (1983) 2375.
26. *Idem*, *ibid.* **16A** (1985) 249.
27. T. OGAWA, K. TOKAJI and K. OHYA, *Fatigue Fracture Engng. Mater. Struct.* **16** (1993) 973.
28. S. V. KAMAT and N. ESWARA PRASAD, *Scripta Metall. Mater.* **26** (1992) 1713.
29. F.-S. LIN and E. A. STARKE, *Mater. Sci. Eng.* **43** (1980) 65.
30. S.-H. WANG and C. MÜLLER, *Fatigue Fracture Engng. Mater. Struct.* **21** (1998) in press.
31. S.-H. WANG, C. MÜLLER and H. E. EXNER, *Metall. Mater. Trans. A* **29A** (1998) 1933.
32. R. C. McCLUNG and H. SEHITOGLU, *Engng Fracture Mech.* **33** (1989) 237.
33. M. F. KANNINEN and C. ATKINSON, *Int. J. Fracture* **16** (1980) 53.
34. T. OGAWA and H. KOBAYASHI, *Fatigue Fracture Engng. Mater. Struct.* **10** (1987) 273.
35. R. O. RITCHIE, W. YU, A. F. BLOM and D. K. HOLM, *ibid.* **10** (1987) 343.

Received 2 March
and accepted 30 June 1998